

Experimental observation of long delay times in the reaction induced by oxygen ions on nickel crystals

E. Fuschini and F. Malaguti

Dipartimento di Fisica and Istituto Nazionale di Fisica Nucleare, Bologna, Italy

E. Fioretto, R. A. Ricci, and L. Vannucci

Laboratori Nazionali di Legnaro, Istituto Nazionale di Fisica Nucleare, Padova, Italy

A. D'Arrigo, G. Giardina, and A. Taccone

Dipartimento di Fisica and Istituto Nazionale di Fisica Nucleare, Messina, Italy

A. Moroni

Istituto Nazionale di Fisica Nucleare, Sezione di Milano, Italy

N. Eremin and O. Yuminov

Nuclear Physics Institute, Moscow State University, Russia

G. Vannini

Dipartimento di Fisica and Istituto Nazionale di Fisica Nucleare, Trieste, Italy

(Received 19 May 1994)

The crystal blocking technique has been used to measure nuclear time delays in the $^{16}\text{O}(135\text{ MeV})+^{\text{nat}}\text{Ni}$ reaction. From the axial blocking patterns the time delays for the production of fragments with Z from 13 to 18 have been extracted. Times of the order of 10^{-18} s for even Z and less than the sensitivity of the method for odd Z have been found. Two interpretations of these findings have been discussed. The first one seems to indicate that nucleus-nucleus dynamics has to be included in simple statistical models to understand the time scale of fusion-fission processes. In the second interpretation, an explicit model for dechanneling shows how the blocking technique can be extended to measure time delays in decay chains.

PACS number(s): 21.10.Tg, 25.70.Gh, 25.70.Jj, 61.80.Mk

I. INTRODUCTION

The crystal blocking technique (CBT), applied to nuclear reactions, allows one to measure an important observable, i.e., the decay time of nuclear systems, and this is of great importance for the comprehension of reaction mechanisms [1]. As known, CBT consists in measuring the angular distribution (blocking dip) around a crystal axis of the products of a nuclear interaction between a crystal target and a beam impinging at an angle θ with respect to the crystal axis.

It should be stressed that CBT can be successfully exploited only if some characteristics of the reaction are known. For instance, if one assumes that the reaction proceeds through the formation of a compound nucleus (CN) moving in the beam direction with a velocity v , the decay products of the CN will originate at a mean distance $s_t = v\tau \sin\theta$ from a row of atoms of the crystal, τ being the mean lifetime of the CN. As the blocking dip depends on the distance s_t , the lifetime of the CN can be measured for τ values ranging from 10^{-19} to 10^{-16} s depending on the values of θ , v , and on the dimensions of the crystal channel.

This is the standard frame within which, in the past, CBT has been used both in light-ion-induced reactions and, more recently, in low-energy heavy-ion reactions, where the reaction mechanism was easily identified, and, therefore, the decay times were assigned. In particular, for heavy-ion (HI) interactions, decay times for fusion evaporation [2-4] and fusion fission [2,3,5-8] have been measured with this technique.

The measured times for fusion-evaporation processes can be explained in the framework of a standard statistical model and considering the whole particle decay chain, not only the last decay. In this respect, the possibility of extracting information on preequilibrium emission from lifetimes measured by CBT [9] is also interesting. In fact, in Ref. [9] it is shown that the preequilibrium emission affects in a significant way the deexcitation times of an evaporating excited system formed by HI Interaction.

It is worthwhile to notice that CBT can be used even in other cases different from the conventional scheme outlined above. For instance, in the work of Gomez del Campo *et al.* [10] CBT allowed to measure the decay time of primary excited fragments produced in the reaction $^{40}\text{Ar}+\text{Ge}$ at 44 MeV/nucleon. In this case, primary excited projectilelike fragments (PLF) produced by a fast

mechanism like abrasion or deep inelastic collision (“primary time” less than 10^{-21} s) suffer a subsequent decay by particle emission after some time delay (“secondary time”) depending on the excitation energy of the PLF. CBT applied to the secondary fragments allows one to measure the secondary mean time, taking into account velocity and angular distribution of the primary fragments. The measurement of the formation time of the secondary fragments provides information about the production mechanism of the primary fragments and about their excitation energy. Coming back to the fusion-fission process, some problems arise in the understanding of light systems formed in HI interactions, where standard liquid drop and statistical models predict a negligible fusion-fission yield with respect to the fusion-evaporation one.

Only recently it has been experimentally established [11,12] that fission is an important process even in very light nuclear systems. These results have been successfully interpreted by statistical model calculations based on the transition-state model and employing saddle-point energies depending from spin and mass asymmetry. This indicates that statistical processes may occur for all HI reactions, regardless of the CN mass, provided that enough angular momentum is brought into the system. Moreover, measurements of our group performed with CBT on the $^{16}\text{O}+^{28}\text{Si}$ and $^{28}\text{Si}+^{28}\text{Si}$ reactions have shown strong time-delay effects for fragments with mass and energy compatible with a fission process [2,3].

The fact that in light systems the fission probability is relatively large and the lifetime relatively long seems to be contradictory. However, as pointed out by Natowitz *et al.* [13], several experimental results on precission multiplicity indicate a large dynamic hindrance of the competition of fission with particle emission. Fission, even from very excited nuclei, is a relatively cold process, which occurs later in the deexcitation cascade. From the theoretical point of view this has been interpreted as a dynamical effect due to nuclear viscosity [14]. Following Siwek-Wilczynska *et al.* [15], the results of time-scale estimates sensitively depend on the assumed dynamical scenario of the nucleus-nucleus collision, and, if dynamics is neglected, the time scales of fusion fission can be underestimated even by more than a factor of 10. A similar interpretation has been invoked to explain the so-called long-lifetime fission component (LLFC) in heavy and very heavy nuclear systems [16]. In conclusion, it seems possible to have both sizable fission probability and long time delays.

For all these reasons it seems to us very fruitful to study the time scale of the fusion-fission process. In this line, we present here an experimental study of the fusion-fission process in medium-light nuclei. We have measured through CBT time delays relative to fragments having masses compatible with a fission process and produced in the $^{16}\text{O}+^{nat}\text{Ni}$ reaction.

The results were first interpreted according to the traditional scheme, that refers to the lifetime of the CN. Then, we attempted an alternative interpretation showing, more generally than in Ref. [10], how CBT can be used to measure the lifetime of excited fragments that decay in flight during their motion inside the crystal.

II. THE EXPERIMENT

A 135-MeV ^{16}O beam from the Tandem-XTU accelerator at LNL Laboratories (Padova) was focused to less than 1 mm in diameter using only magnetic steering and no collimators. This was necessary to preserve the angular resolution of the experiment without introducing “slit-scattering” effects. The focusing was achieved with magnets very far upstream the target, in order to minimize beam divergence.

Targets were thin ($\sim 0.5 \mu\text{m}$), self-sustaining and large-area ($\Phi \approx 5 \text{ mm}$) $^{nat}\text{Ni}\langle 100 \rangle$ crystals prepared at the Physics Institute, Århus University (Dk). They were epitaxially grown by evaporation on NaCl crystals and mounted on a suitable Ni frame after dissolving the substrate in water. This technique ensured a nearly perfect orthogonality between the crystal axis ($\langle 100 \rangle$) and its surface.

A six-axis computerized goniometer was used to change and orientate the crystals, and to translate them to “fresh” positions after an approximately 60- μC beam dose. No appreciable radiation damage was observed under this fluence: on the contrary, crystal quality seemed to improve in some cases, indicating an unexpected self-annealing phenomenon.

Reaction products were observed at $\theta_{\text{lab}} = 20^\circ$ using a detector telescope consisting of a multiwire counter followed by an axial Bragg chamber. The multiwire detector, $10 \times 10 \text{ cm}^2$ area and placed at a 1-m distance from the target, was a two-sector gas proportional counter with a common (1- μm -thick) cathode and two anodes formed by wires orthogonal to each other. The anodes were at opposite sides of the cathode, and the wires (20 μm diam) were at 1 mm away. Gas (isobutane) pressure was 18 mbar under continuous flux, and total detector thickness was 5 mm. The Bragg chamber was an ionization chamber operating with an axial electric field and at a gas (CF_4) pressure of 55 mbar. In this way fragments with atomic number $Z > 12$ were stopped in the chamber allowing to measure their energy and, from the Bragg peak, also Z . The energy resolution was better than 1.5%.

Crystal and telescope orientation were made very easy by the orthogonality between the $\langle 100 \rangle$ axis and the target surface. We simply rotated the target at the same angle with respect to the beam as the detector (20°), and this always allowed us to see the blocking pattern within the multiwire. Then we used the goniometer to achieve perfect orientation. All that was done “online” using the beam just before experiment and made prealignment unnecessary. Events, defined by the x, y spatial coordinates of the ion from the multiwire and by its kinetic energy E and charge Z from the Bragg chamber, were collected individually on magtape for offline data reduction.

Figure 1 shows a scatter plot from the Bragg chamber: all data are shown here, with no cut on $x-y$ values. One sees that individual Z values are resolved up to 16. Fragments with $Z > 16$ were assumed in the analysis to have $Z=18$.

Besides the main measurements on the reaction ^{16}O (135 MeV) + $^{nat}\text{Ni}\langle 100 \rangle$ we performed additional short

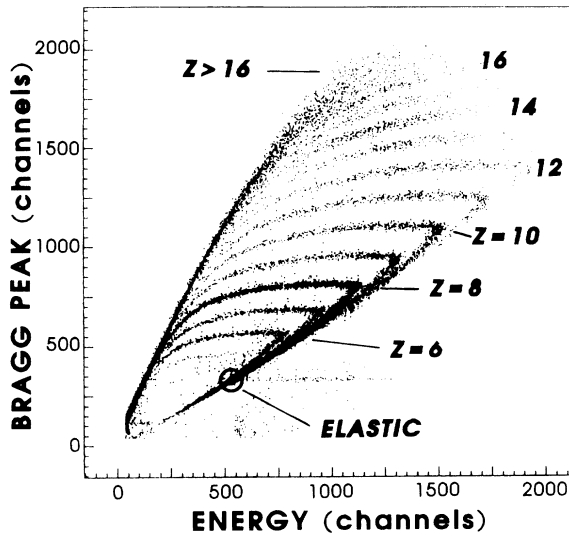


FIG. 1. Scatter plot from the Bragg chamber: height of the Bragg peak vs ion kinetic energy. The experimentally resolved Z values are also shown. The beam was ^{16}O (135 MeV) on a ^{nat}Ni crystal; $\theta_{\text{lab}} = 20^\circ$. The data shown here are for all x, y values.

measurements to check the crystal quality, the angular resolution, and the scaling law (see Sec. III) for different Z values. They were done using subbarrier elastic scattering of ^{32}S ions ($E=53.5$ and 124.2 MeV) and of ^{16}O ions ($E=57.4$ MeV) on the Ni crystals.

As an example, Fig. 2 displays a scatter plot from the multiwire detector, showing a two-dimensional blocking pattern (left), together with the radial scan around its center (right). These additional measurements demonstrate both the crystal quality and the angular resolution of the experiment (≈ 1 mrad).

Figure 3 displays typical energy spectra of fragments emitted in the ^{16}O (135 MeV) + $^{nat}\text{Ni}(100)$ reaction. The spectra of "fissionlike" fragments with resolved Z (13–16) are nearly identical, and all peak around the energy corresponding to Coulomb repulsion. The low-energy shape of the spectrum for unresolved Z (> 16) is due to the mixing of different Z 's and different nuclear processes.

III. ANALYSIS AND RESULTS

Data analysis consisted in constructing the blocking dip for each detected Z (see Fig. 4 as an example) and in measuring the ratio $R = \Omega_D/\Omega_P$ between its delayed volume Ω_D and the corresponding volume Ω_P of the elastic (prompt) dip [2]. This is a simple observable sensitive to time delay and nearly independent from crystal defects.

In principle, delayed and prompt dip volumes should be measured for the same values of E and Z but, following Refs. [2,17], one can exploit a charge-energy scaling law and define a "reduced volume"

$$\Omega^* = \Omega \langle E^{-1} \rangle^{-1} / Z \quad (1)$$

that is independent from E and Z and can be used in place of Ω .

The validity of the scaling law has been verified for Ni(100) crystals measuring volumes of elastic blocking dips obtained in the additional measurements with the ^{32}S beam ($E=53.5$ and 124.2 MeV), and with the ^{16}O beam (57.4 MeV), together with elastic volumes obtained simultaneously with the lifetime experiment. While dip volumes were very different, their reduced values clustered around the weighted mean

$$\Omega_P^* = 520 \pm 7 \text{ MeV } \mu\text{sr} \quad (2)$$

and were found consistent (at the 5% level) using a χ^2 test.

We have analyzed fragments ranging from $Z = 13$ to $Z > 16$, and the experimental values for $\langle E^{-1} \rangle^{-1}$, Ω_D^* , and R are collected in the third, fourth, and fifth rows of Table I. To Ω_P was given the value (2). All errors quoted here and in the table are only statistical. $Z = 11$ and 12 were also considered, but the results are not displayed here as they probably suffer contamination from C and O on the target.

We assumed $Z=18$, while calculating Ω_D^* for $Z > 16$ fragments, but this should not significantly affect the results of the present work. In fact, a one- or two-unit change in Z does not appreciably influence the reduced volume (1). Moreover, increasing Z over 20 would decrease Ω_D^* , hence increase even more the lifetimes dis-

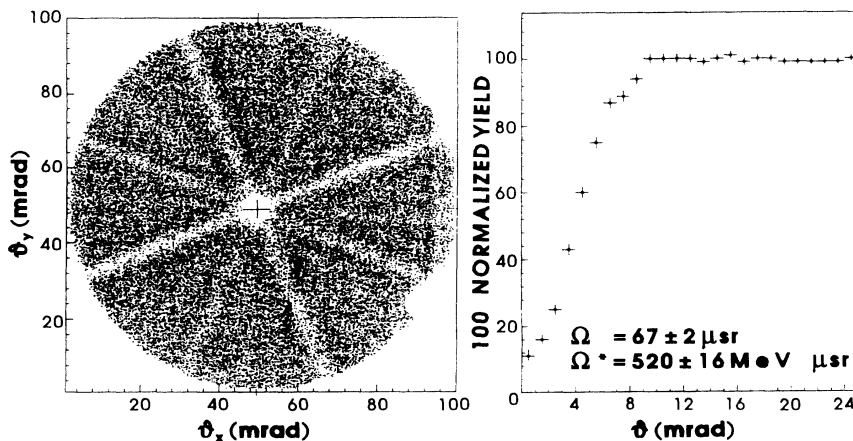


FIG. 2. Example of elastic (prompt) blocking dip, due to ^{32}S ions (124.2-MeV kinetic energy) on a Ni(100) crystal, 0.5 μm thick. Left: x - y scatter plot from the multiwire detector. Right: radial scan around the dip center.

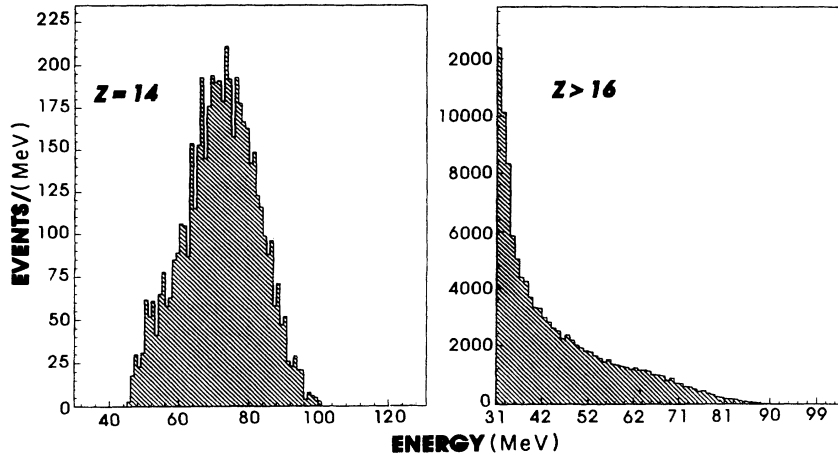


FIG. 3. Energy spectra. Left: $Z=14$ (one of the resolved Z 's); all spectra of this kind are very similar. Right: unresolved part of the scatter plot (see Fig. 1).

played in the table for $Z > 16$. From the table we see $R < 1$, i.e., a time delay effect, in some cases ($Z=14, 16$, $Z > 16$ and $E < 60$ MeV), while R is compatible with 1, i.e., nonmeasurable time delay, for $Z=13, 15$, $Z > 16$ and $E > 60$ MeV.

In the traditional interpretation of blocking experiments [1], the lifetime effect is ascribed to the CN that recoils due to the impulse received from the projectile. The shape of the dip depends from the distribution of transverse displacements x_t traveled by the CN before decay, hence, for exponential decay, from

$$s_t = \langle x_t \rangle = \text{transverse velocity} \times \text{mean life of the CN} . \quad (3)$$

One can use the theory of ion motion within crystals [18] to calculate the dependence of the experimental parameter R from s_t . This has been done using a Monte Carlo method [19] and the result is displayed in Fig. 8(a). We used this "calibration curve" to extract s_t values and the corresponding lifetimes from R .

The results are shown in the sixth and seventh rows of Table I. As it can be seen, the main outcome is that fragments with even Z are emitted with a sizeable time delay, whereas the odd ones seem to be prompt. Moreover, the $Z > 16$ fragments present a time delay only for energies corresponding to higher relaxation.

IV. DISCUSSION

Neglecting the presence of this odd-even effect, that could be statistically not very significant, the standard interpretation of the experimental data would indicate a lifetime $\tau \approx 3$ as for compound systems in the region of the Kr nucleus around 100-MeV excitation energy. This result disagrees with the predictions of a standard statistical model described in more details in Appendix A. Calculated lifetimes of excited Kr nuclei produced in this reaction are largely dominated by particle emission and are of the order 10^{-20} to 10^{-21} s. In this model, the result is essentially left unchanged if fission after evaporation of some particles is assumed. In fact, if the CN excitation energy decreases, the number of channels open for fission falls down more quickly than that for particle decay, so that fission becomes unlikely, while particle emission still is dominating and the CN global lifetime remains about 10^{-19} to 10^{-20} s.

As already mentioned in the Introduction, it should be stressed [15] that statistical models that do not consider dynamical effects are inadequate to describe the whole fusion-fission process [20], and can underestimate the fission time scale by more than a factor of 10. On the other hand, it should also be noticed that a recent measurement with a new interferometry technique [21] gives, as an average over a five-neutron evaporation cascade:

TABLE I. Summary of experimental results. ΔE (and $\langle E^1 \rangle^{-1}$) (MeV) are the interval of kinetic energies (and the corresponding mean inverse energy). Ω_D^* (MeV μsr) is the "reduced" dip volume, and $\Omega_P^* = 520 \pm 7$ its "prompt" value. s_t and s_L (\AA) are the transverse and longitudinal mean displacements for exponential decay, while τ_1 and τ_2 (as $=10^{-18}$ s) are the corresponding primary and secondary mean times.

Z	13	14	15	16	> 16	> 16	> 16
ΔE	40-110	45-100	45-95	50-95	40-50	50-60	>60
$\langle E^{-1} \rangle^{-1}$	70.8	69.9	69.7	70.0	44.4	54.6	68.2
Ω_D^*	557 ± 105	418 ± 68	497 ± 107	393 ± 66	446 ± 37	454 ± 43	507 ± 68
$R = \Omega_D^* / \Omega_P^*$	1.07 ± 0.20	0.80 ± 0.13	0.96 ± 0.21	0.76 ± 0.13	0.86 ± 0.07	0.87 ± 0.08	0.98 ± 0.13
s_t	≈ 0 (< 0.08)	$0.10^{+0.95}_{-0.94}$	≈ 0 (< 0.12)	$0.12^{+0.06}_{-0.05}$	0.08 ± 0.02	0.08 ± 0.03	≈ 0 (< 0.08)
τ_1	≈ 0 (< 2.7)	$3.4^{+1.7}_{-1.4}$	≈ 0 (< 4.1)	$4.1^{+2.0}_{-1.7}$	2.7 ± 0.7	2.7 ± 1.0	≈ 0 (< 2.7)
s_L	≈ 0 (< 0.7)	$1.1^{+0.6}_{-0.7}$	≈ 0 (< 1.3)	1.3 ± 0.7	0.7 ± 0.4	0.7 ± 0.4	≈ 0 (< 0.8)
τ_2	≈ 0 (< 3.0)	$5.0^{+2.7}_{-3.2}$	≈ 0 (< 6.1)	6.3 ± 3.4	4.5 ± 2.6	4.1 ± 2.3	≈ 0 (< 4.2)

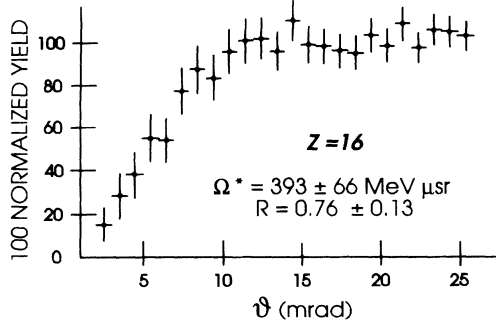


FIG. 4. Experimental blocking dip for the inelastic reactions leading to $Z=16$ fragments. Radial scan around the dip center, reduced volume Ω^* and R value.

$$\tau \leq (1.2 \pm 0.1) \times 10^{-20} \text{ s}$$

for the nearby nucleus ^{82}Kr ($E^*=88$ MeV).

This finding agrees with the predictions of the statistical model for the fission-evaporation process of Kr nuclei, and does not disagree with our result, which indeed refers to the time scale of the whole fusion-fission process. However, to explore alternative interpretations, we discuss in the next sections the possibility that the time delays measured in the present experiment can be due to a secondary effect.

In this respect our interest is to study, on a general ground, the change produced to blocking dips by in-flight decay of the reaction products. We do it focusing our attention particularly to the case of $Z = 16$ fragments.

A. Dechanneling due to in-flight decay of the observed fragment and extraction of secondary delay times

As pointed out by Karamyan [22] and by Hoernle', Fearick, and Sellshop [23], in heavy-ion blocking experiments the detected fragment is an excited nucleus that can decay in flight by γ or particle emission. The random impulse imparted to the fragment by the emitted particle produces a "smearing" of the blocking dip (dechanneling) that simulates a lifetime effects.

A beautiful example of this phenomenon has been observed [23] in the scattering of ^{12}C (31.2 MeV) on a $^{28}\text{Si}(110)$ crystal. Here carbon ions coming from elastic scattering or from inelastic scattering to the 1.78 MeV level of $^{28}\text{Si}^*$ produce a typically "prompt" blocking pattern, very deep and "empty." On the other hand, carbon ions from inelastic scattering to the 4.43-MeV level of $^{12}\text{C}^*$ display a nearly completely "filled-in" blocking dip. The reason is not time delay, but dechanneling due to γ -decay of the excited $^{12}\text{C}^*$ ions in flight. A theory of the phenomenon has been given in the framework of the continuum model for channeling [18], distinguishing γ decays inside the crystal, where the transverse energy changes as during scattering by a point defect and γ decays outside the crystal, which can be described as a simple convolution over the unperturbed blocking dip.

Clearly the dechanneling effect we have just described has to be accounted for in the interpretation of crystal blocking experiments. While it is certainly very dangerous if one wants to measure the lifetime of the compound nucleus (primary time), it is interesting to observe that it can be used as a variant of the blocking method to measure the lifetime of the fission fragments (secondary time). The idea, which was proposed by Karamyan [22] and by J. Gomez del Campo *et al.* [10], is illustrated in Fig. 5.

The beam interacts with a lattice atom producing a compound nucleus whose primary lifetime is assumed for simplicity $\tau_1 \approx 0$, i.e., below the sensitivity limit of the blocking method. The CN splits into excited fission fragments (FF) that eventually decay in flight after a secondary mean time τ_2 . Distribution of recoil angles ψ can be calculated from reaction kinematics and introduced within our Monte Carlo code for channeling [19].

Assuming isotropic emission from the FF, and small angles of deflection, the probability density for ψ is [23]

$$f(\psi) = \frac{\psi/\psi_m}{(\psi_m^2 - \psi^2)^{1/2}}, \quad \psi \in [0, \psi_m] \quad (4)$$

where the maximum deviation angle ψ_m is given by

$$\psi_m^2 = E_\gamma^2 / (2Mc^2T) \quad (5)$$

for gamma decay, or

$$\psi_m^2 = M_P T_P / MT \quad (6)$$

for particle decay. Here, M and T (M_P and T_P) are mass and kinetic energy of the FF (emitted particle), respectively.

Deflection angles ψ can easily be sampled as

$$\psi = \psi_m \sqrt{1 - \text{Ran}^2}, \quad (7)$$

where Ran is a uniform $[0,1]$ variate. They can be introduced in the full three-dimensional Monte Carlo simulation together with the azimuthal angle χ that is assumed

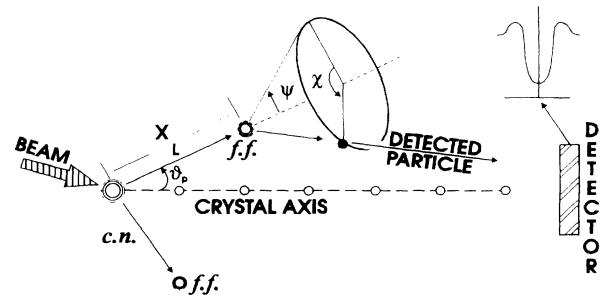


FIG. 5. Geometrical relationships for secondary particle dechanneling. The compound nucleus (CN) is assumed to have a negligible lifetime ($\tau_1 = 0$), and x_L is the longitudinal path traveled by the fission fragment (FF) before decay. The angles ψ and χ define the new particle direction after in-flight decay.

uniform over $[-\pi, +\pi]$. In this way, a new direction of propagation is generated for the FF, whose subsequent path is calculated in the usual way [19].

Clearly, the effect on the whole blocking pattern will depend on the distribution of distances x_L traveled along its path by the FF before decay, hence, for exponential decay, on the longitudinal mean displacement

$$s_L = \langle x_L \rangle = \text{velocity} \times \text{mean life of the FF} . \quad (8)$$

In particular, if $s_L=0$, the blocking pattern is left unchanged. In fact, the angular distribution of FF due to decay has to be convoluted with the one before decay, that is initially isotropic (and therefore remains isotropic) for small angles around the crystal axis.

If now s_L increases, the originally isotropic distribution evolves towards the blocking pattern, that is reached after passing some tenths of crystal planes. Correspondingly, the dechanneling effect due to in-flight decay grows bigger and bigger, and so the modification on the final blocking pattern.

Detailed calculations performed with the Monte Carlo code have shown that the way the blocking pattern is affected depends strongly on the maximum deflection angle ψ_m , Eqs. (5) and (6). For moderate deflection angles (like those due to γ decay), say

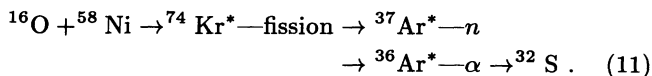
$$\psi_m \approx \psi_L \text{ (Lindhard's angle) } , \quad (9)$$

the blocking dip fills up, but it enlarges also, so that the dip volume is left unchanged. Figure 6 displays some calculations performed for the reaction studied in Ref. [23]: (a) is a reference (elastic) dip compared with a calculation for a large longitudinal displacement (b). In spite of the strongly different shapes, the two dips have the same volume. Of course the volume still depends on the transverse displacement (primary time τ_1) as case (c) demonstrates.

Therefore, if ψ_m is moderate, the method of analysis of blocking experiments based on the dip volume is still sensitive to the primary time, and is not perturbed by dechanneling due to secondary decay. The situation becomes very different if ψ_m is large (like in the case of alpha decay), viz.,

$$\psi_m \gg \psi_L . \quad (10)$$

Figure 7 displays simulations relative to the reaction $^{16}\text{O} + \text{Ni}(100)$ studied in this work. Case (a) is an elastic blocking dip due to ^{32}S ions having 70-MeV kinetic energy (measured value for $Z=16$ fragments). A possible channel for their formation could be



Assuming $T_\alpha=10$ MeV (a theoretical guess based on statistical model) we get a maximum recoil angle $\psi_m=130$ mrad, to be compared with Lindhard's angle $\psi_L=7.23$ mrad. A corresponding calculated blocking dip is case (b) of Fig. 7: not only is the shape modified, but also its width, and therefore its volume, are reduced.

This means that now the method of analysis based on the volume is sensitive both on primary and on secondary time, that together contribute to the filling in of the blocking dip.

B. A possible interpretation of the O+Ni data in terms of secondary time

The discussion contained in the preceding section suggests an alternative interpretation of the present experiment. Having particularly $Z=16$ fragments in mind, we consider their possible formation channel given by Eq. (11). In cases like this, the observed ion is originated by a fission fragment undergoing a decay chain whose last particle step is α decay. It therefore suffers strong recoil and dechanneling during its passage through the crystal.

To consider an extreme case, let us assume that all observed ions come from a secondary α decay, and that the CN (primary) lifetime τ_1 is below the lowest sensitivity limit of the blocking method. In this case, the volume of

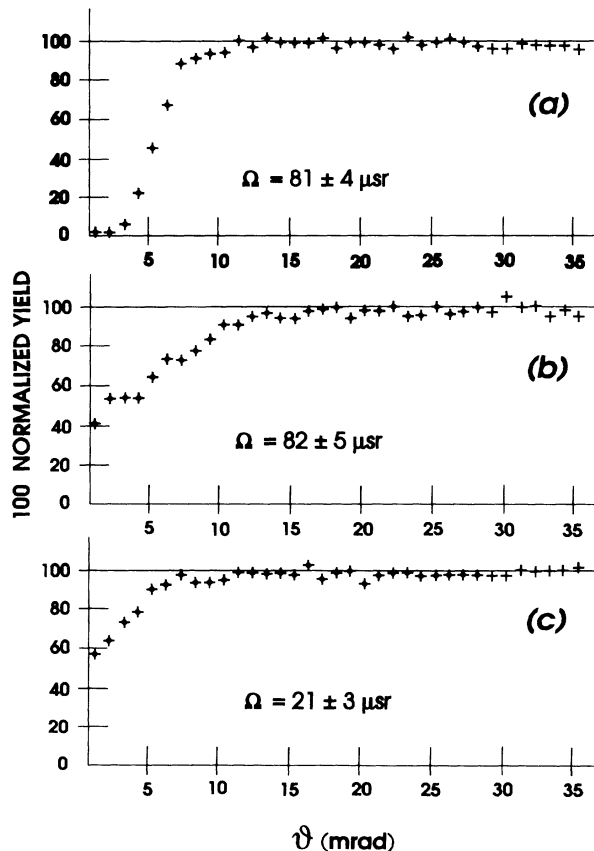


FIG. 6. Monte Carlo simulations for the process studied in Ref. [23]: ^{12}C ions (23.6-MeV kinetic energy) on a $^{28}\text{Si}(100)$ crystal, $0.57 \mu\text{m}$ thick. Lindhard's angle was $\psi_L=5.17$ mrad. Case (a) refers to elastic scattering (no recoil), while case (b) corresponds to longitudinal recoil (secondary time) with a $3000\text{-}\text{\AA}$ mean displacement and maximum deflection angle $\psi_m = 6.1$ mrad. Case (c) was calculated assuming transverse recoil (primary time) with mean displacement of 0.8\AA .

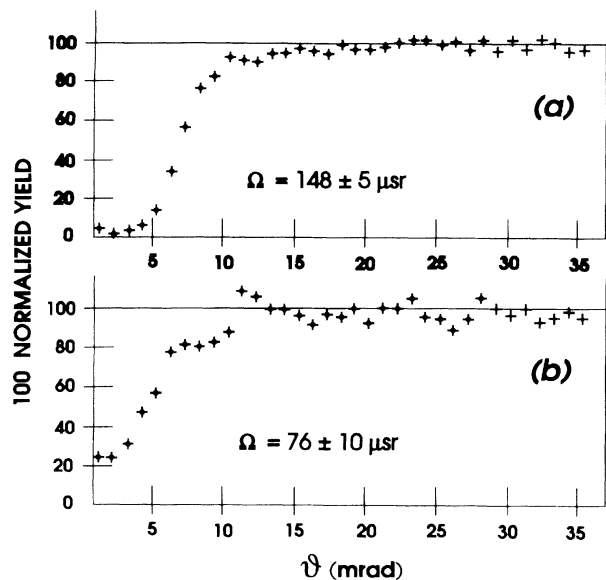


FIG. 7. Monte Carlo simulations for the process studied in the present work: ^{32}S ions (70-MeV kinetic energy) on a Ni(100) crystal, $0.25\ \mu\text{m}$ thick. Lindhard's angle is $\psi_L=7.23$ mrad. Case (a) refers to elastic scattering (no recoil), while case (b) corresponds to longitudinal recoil (secondary time) with $3\text{-}\text{\AA}$ mean displacement and maximum deflection angle $\psi_m=130$ mrad.

the blocking dip is sensitive only to the secondary time τ_2 of this α decay, and one can use the Monte Carlo code to calculate the appropriate calibration curve $R(s_L)$.

Assuming again $T_\alpha=10$ MeV, therefore $\psi_m=130$ mrad, we compare in Fig. 8(b) the new calibration curve $R(s_L)$ with the one (a) obtained in the traditional interpretation (primary time). See Appendix B for a further discussion about the relation between the two curves. The corresponding s_L and τ_2 extracted from experimental R values are collected in the eighth and ninth rows of the table for all observed fragments.

These outcomes rely on the statistical model estimate $T_\alpha=10$ MeV, but the assumption is absolutely not critical. Another calibration curve (not shown here) was calculated for $T_\alpha=5$ MeV ($\psi_m=90$ mrad) and resulted in the same τ_2 values within experimental errors. The reason is that the appropriate calibration curve is very similar to that of Fig. 8(b) for $R > 0.7$.

The present results can be compared with the statistical model described in Appendix A calculating the nuclear lifetime for $^{36}\text{Ar}^*$ at 18-MeV excitation energy, sufficient to allow α decay and to produce therefore a ^{32}S detected fragment. The result is about 2.7×10^{-18} s, in good agreement with our findings.

Of course this interpretation of the data is simplified because it neglects the contribution of neutron, proton, and γ emission before the formation of the observed fragments, so that the quoted numbers are only indicative, and should be interpreted as averages over all possible formation channels. It is nevertheless interesting to observe that τ_1 and τ_2 values in the table, though coming

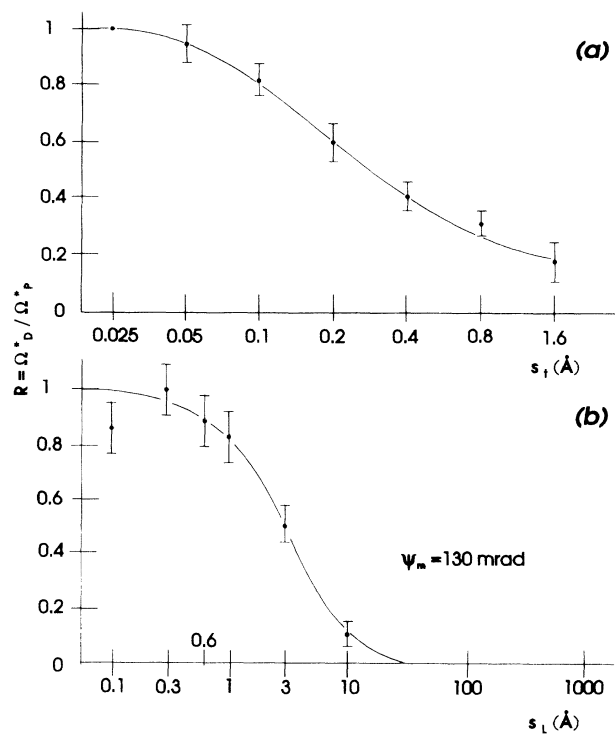


FIG. 8. Calibration curves $R(s_t)$ and $R(s_L)$ calculated with the Monte Carlo method for a Ni(100) crystal, $0.25\ \mu\text{m}$ thick. Case (a) corresponds to the traditional interpretation, where s_t =transverse velocity \times mean life (compound nucleus). Case (b) refers to the interpretation in terms of secondary time, where s_L =velocity \times mean life (fission fragment). In both cases we assumed exponential decay. The continuous curves are visual fits to the data.

from so different views, differ only by a factor ≈ 1.5 .

They correspond to two extreme cases, related to the "primary" and "secondary" times. All other possible cases, such as, for instance, an evaporation chain ending in a fission, produce decay times included between these two extremes. Anyway, CBT allows us in all cases to measure the nuclear time delay associated with fragment formation. Moreover, in-flight decay, instead of being a difficulty, reveals itself as a further challenging possibility offered by the method; see also Appendix B.

V. CONCLUSIONS

We have measured time delays in the nuclear reaction induced by ^{16}O ions (135 MeV) on $^{nat}\text{Ni}(100)$ crystals using the blocking method. Experimental data show time-delay effects, ranging between 3 and 6×10^{-18} s, for $Z=14,16$ and for $Z > 16$, $T < 60$ MeV (high-energy relaxation), while they are compatible with zero in the other cases. The effect of in-flight dechanneling on the experiment has been considered qualitatively by means of a Monte Carlo calculation for ion motion within crystals.

A combined analysis of experimental data and of dechanneling calculations has been performed under two

extreme hypotheses. The primary one interprets the observed filling-in of the blocking dips as due to time delay in the fission process of the compound nucleus, even in the presence of precission emission of light particles. This seems to indicate that nucleus-nucleus dynamics has to be included in simple statistical models to understand the time scale of fusion-fission processes. The secondary scheme, on the contrary, sees the effect as due to the time delay associated with α decay in the deexcitation chain of the fission fragment, and seems to agree with standard statistical model calculations of its lifetime.

To distinguish which reaction mechanism is responsible for the filling-in of the blocking dip, it would be useful to perform different measurements changing the angle θ between the beam and the crystal axis, and the beam energy, as well. A further improvement would be to observe the blocking pattern of the fragment in coincidence with the emitted light particles. In this way, one could understand whether the CN or the fission fragment is the source of the light particle.

ACKNOWLEDGMENTS

We are deeply indebted to Jacques Chevallier and the Physics Institute of Århus University for having prepared the thin Ni(100) crystals. The strong support of the Tandem-XTU staff and the technical cooperation of Danilo Bulgarelli and Alessandra Spada have also been of invaluable help.

APPENDIX A: STATISTICAL MODEL CALCULATION

In order to evaluate nuclear lifetimes, we used an appropriate statistical model code [24–26] based on the Hauser-Feshbach theory including heavy-ion-induced fission. Special attention has been devoted to the treatment

of the level densities (in the cases of yrast shapes for the particle emission channels, and at the saddle-point configuration for the fission process) for prolate and oblate nucleus deformations. For the level density parameter a we used Ignatyuk's well-known formula [27], which was especially tailored to account for shell effects in the level density.

Moreover, collective effects in the nonadiabatic approach were considered in the level density, and also the effects related to the nuclear shapes, which undergo the dynamical evolution with increasing spin. In the present calculations we considered up to the fourth-chance fission allowing for the competition of neutron, proton, and α emission. In the cases of the second-, third-, and fourth-chance fission, we also account for the full γ cascade, since at lower energies it may effectively compete with the particle emission and fission channels. It was observed that the fission process is extremely sensitive to angular momentum, therefore other parameters of crucial importance are moments of inertia that determine spin distribution of the levels. In the case of the saddle-point configuration the three principal moments of inertia were obtained by means of Sierk's routine BARMON [28], which agrees with the results of the advanced rotating liquid drop model (RLDM) calculations. The moments of inertia from the yrast states were calculated by the β - and γ -deformation parameters using formulas reported in the Appendix of Ref. [29]. The spin-dependent fission barriers were obtained using the BARFIT routine [28] based on the same RLDM calculations that also provided moments of inertia, and the shell correction to the fission barrier was also considered, even if the shell effect is small with respect to the macroscopic barrier height of $^{74,76}\text{Kr}$. Therefore, because of the high macroscopic barrier, we disregarded the dynamical effects related to dissipation and fluctuations of the collective nuclear motion. The lifetime of an excited nucleus was evaluated by means of the fission and particle decay widths as described in Ref. [24]

$$\Gamma_f(E, J, \pi) = \frac{1}{2\pi\rho_{\text{CN}}(E, J, \pi)} \int_0^{E-E_{\text{sad}}(J)} \rho_f(E - E_{\text{sad}}(J) - \varepsilon, J, \pi) T_f(E - \varepsilon) d\varepsilon ,$$

$$\Gamma_x(E, J, \pi) = \frac{1}{2\pi\rho_{\text{CN}}(E, J, \pi)} \sum_{J'=0}^{\infty} \sum_{\pi'} \sum_{j=|J'-J|}^{J'+J} \int_0^{E-B_x} \rho_x(E - B_x - \varepsilon, J', \pi') T_x^{l,j}(\varepsilon) d\varepsilon .$$

The total width Γ_{tot} was obtained by operating a weighted average of the above-mentioned decay widths over all spin states, which leave the nucleus at an effective excitation energy higher than the fission barrier. Hence, the nuclear lifetime is obtained by the relation $\hbar/\Gamma_{\text{tot}}$.

Starting from the $^{74,76}\text{Kr}$ compound nucleus and considering various decay chains that produce fission after

neutron, proton, or α emission, we find nuclear lifetimes ranging between 5×10^{-20} s (for $^{71,73}\text{As}$), 7×10^{-21} s (for $^{66,68}\text{Ge}$) and up to 0.5×10^{-21} s (for the $^{74,76}\text{Kr}$ compound nucleus) at the excitation energy related to the ^{16}O (135 MeV) + $^{\text{nat}}\text{Ni}$ reaction.

Moreover, concerning the possible excited fission fragments produced by the above-mentioned reaction and that decay via neutron or alpha particle, we calculate

a nuclear lifetime of about 2.7×10^{-18} s, e.g., for $^{36}\text{Ar}^*$ at 18-MeV excitation energy, sufficient to allow α decay and to produce, therefore, a ^{32}S -detected fragment.

APPENDIX B: RELATION BETWEEN PRIMARY AND SECONDARY TIME-CALIBRATION CURVES

Let us call here $R_1(s_1)$ and $R_2(s_L)$ the primary and secondary calibration curves displayed in Fig. 8. From the figure we see that they are very similar, apart from a scale transformation in the abscissa. With reference to Fig. 5, this can be easily understood observing that only secondary trajectories beginning nearly parallel to the crystal axis can contribute to the blocking dip. This happens only if the angle between the velocity of the primary fragment and the axis $\theta_P \approx \psi$, and $\chi \approx \pi$. But the distribution of ψ , see Eq. (4), having a mean value

$$\langle \psi \rangle = \frac{\pi}{4} \psi_m = 0.7854 \psi_m \quad (\text{B1})$$

and a standard deviation 3.5 times smaller,

$$\sigma(\psi) = \sqrt{2/3 - \pi^2/16} \psi_m = 0.2232 \psi_m, \quad (\text{B2})$$

is strongly peaked near its mean value. Therefore, relevant trajectories satisfy the condition

$$\theta_P \approx \langle \psi \rangle = 0.7854 \psi_m, \quad (\text{B3})$$

as though we were observing primary decay with an angle $\approx 0.7854 \psi_m$ between the beam and the crystal axis. The corresponding x_t would be $x_L \sin(0.7854 \psi_m)$, and we can conclude that

$$\text{if } s_t = s_L \sin(0.7854 \psi_m) \text{ then } R_1(s_t) \approx R_2(s_L). \quad (\text{B4})$$

Of course this is a very crude argument because the relevant angles (B3) are allowed to differ by Lindhard's angle and because (B4) can be applied only if the trajectory between primary and secondary decay is rectilinear, which requires an $s_L \leq$ lattice distance. Anyway, Fig. 8 shows that is approximately correct, being $\sin(0.7854 \psi_m) = 0.10$.

-
- [1] W. M. Gibson, *Annu. Rev. Nucl. Sci.* **25**, 465 (1975); I. Massa and G. Vannini, *Riv. Nuovo Cimento* **5**, 9 (1982).
- [2] F. Malaguti, S. Ostuni, E. Verondini, E. Fuschini, G. Vannini, I. Iori, A. Bracco, A. Moroni, E. Fioretto, R. A. Ricci, P. Boccaccio, and L. Vannucci, *Nuovo Cimento A* **101**, 517 (1989); *Europhys. Lett.* **12**, 313 (1990).
- [3] E. Fuschini, F. Malaguti, S. Ostuni, E. Verondini, G. Vannini, E. Fioretto, R. A. Ricci, P. Boccaccio, L. Vannucci, A. D'Arrigo, G. Giardina, and A. Taccone, *Phys. Rev. C* **46**, R25 (1992).
- [4] J. Gomez del Campo, D. Shapira, J. A. Biggerstaff, C. D. Moak, P. D. Miller, N. Neskovic, R. W. Fearick, and J. P. F. Sellshop, *Phys. Rev. Lett.* **51**, 451 (1983).
- [5] J. Gomez del Campo, *Nucl. Instrum. Methods Phys. Res. Sect. B* **24**, 447 (1987).
- [6] J. U. Andersen, A. S. Jensen, K. Jorgensen, E. Laegsgaard, K. O. Nielsen, J. S. Forster, I. V. Mitchell, D. Ward, W. M. Gibson, and J. J. Cuomo, *K. Dan. Vidensk. Selsk. Mat. Phys. Medd.* **40**, 1 (1980).
- [7] J. S. Forster, I. V. Mitchell, J. U. Andersen, A. S. Jensen, E. Laegsgaard, W. M. Gibson, and K. Reichelt, *Nucl. Phys. A* **464**, 497 (1987).
- [8] N. Bugrov and S. A. Karamyan, *Yad. Fiz.* **35**, 558 (1982) [*Sov. J. Nucl. Phys.* **35**, 322 (1982)].
- [9] R. Bonetti and C. Chiesa, *Mod. Phys. Lett.* **5**, 619 (1990).
- [10] J. Gomez del Campo, J. Barrette, R. A. Dayras, J. P. Wieleczko, E. C. Pollacco, S. Saint-Laurent, M. Toulemonde, N. Neskovic', and R. Oistojic', *Phys. Rev. C* **41**, 139 (1990).
- [11] S. J. Sanders, B. B. Back, R. V. F. Janssens, D. G. Kovar, D. Habs, D. Henderson, T. L. Khoo, H. Korner, G-E. Rathke, T. F. Wang, F. L. H. Wolfs, and K. B. Beard, *Phys. Rev. C* **41**, R1901 (1990).
- [12] R. M. Anjos, N. Added, N. Carlin, L. Fante, Jr., M. C. S. Figueira, R. Matheus, H. R. Schelin, E. M. Szanto, C. Tenreiro, A. Szanto de Toledo, and S. J. Sanders, *Phys. Rev. C* **48**, R2154 (1993).
- [13] J. B. Natowitz, M. Gonin, M. Gui, K. Hagel, Y. Lou, D. Utley, and R. Wada, *Phys. Lett. B* **247**, 242 (1990).
- [14] K. H. Bhatt, *Phys. Rev. C* **33**, 954 (1986).
- [15] K. Siwek-Wilczynska, J. Wilczynski, H. K. W. Leegte, R. H. Siemssen, H. W. Wilshut, K. Grotowski, A. Panasiewicz, Z. Sosin, and A. Wieloch, *Phys. Rev. C* **48**, 228 (1993).
- [16] N. D. Mavlitov, P. Frobrich, and I. I. Gontchar, *Z. Phys. A* **342**, 195 (1992); Yu. A. Lazarev, I. I. Gontchar, and N. D. Mavlitov, Report No. HMI 1992/P1-Laz 1.
- [17] F. Malaguti, S. Ostuni, E. Verondini, E. Fuschini, G. Vannini, I. Iori, and A. Moroni, *Nuovo Cimento A* **104**, 1211 (1991).
- [18] J. Lindhard, *K. Dan. Vidensk. Selsk. Mat. Fys. Medd.* **34**, n.4 (1965).
- [19] F. Malaguti, *Nucl. Instrum. Methods Phys. Res. Sect. B* **34**, 157 (1988).
- [20] D. Hilscher, *Ann. Phys. (Paris)* **17**, 471 (1992).
- [21] R. Gentner, K. Keller, W. Luecking, and L. Lassen, *Z. Phys. A* **343**, 401 (1992).
- [22] S. A. Karamyan, *Nucl. Instrum. Methods Phys. Res. Sect. B* **51**, 534 (1990).
- [23] R. F. A. Hoernle', R. W. Fearick, and J. P. F. Sellshop, *Phys. Rev. Lett.* **68**, 500 (1992).
- [24] A. D'Arrigo, G. Giardina, M. Herman, and A. Taccone, *Phys. Rev. C* **46**, 1437 (1992).
- [25] A. D'Arrigo, G. Giardina, M. Herman, A. V. Ignatyuk, and A. Taccone, *J. Phys. G* **20**, 365 (1994).
- [26] A. D'Arrigo, N. V. Eremin, E. Fioretto, E. Fuschini, G. Giardina, F. Malaguti, A. Moroni, R. A. Ricci, M. Sacchi, A. Taccone, G. Vannini, L. Vannucci, and O. A. Yuminov, in *Proceedings of the International Symposium on Time Characteristics of Nuclear Reactions, Moscow, 1993*, edited by N. V. Eremin and O. A. Yuminov ("Print", Moscow State University, 117463 Moscow, 1994).
- [27] A. V. Ignatyuk, G. N. Smirenkin, and A. S. Tishin, *Yad. Fiz.* **21**, 485 (1975) [*Sov. J. Nucl. Phys.* **21**, 255 (1975)].
- [28] BARMON, No. 9677, National Energy Software Center, Argonne National Laboratory, Argonne, IL 60439.
- [29] S. E. Vigdor and H. J. Karwowski, *Phys. Rev. C* **26**, 1068 (1982).

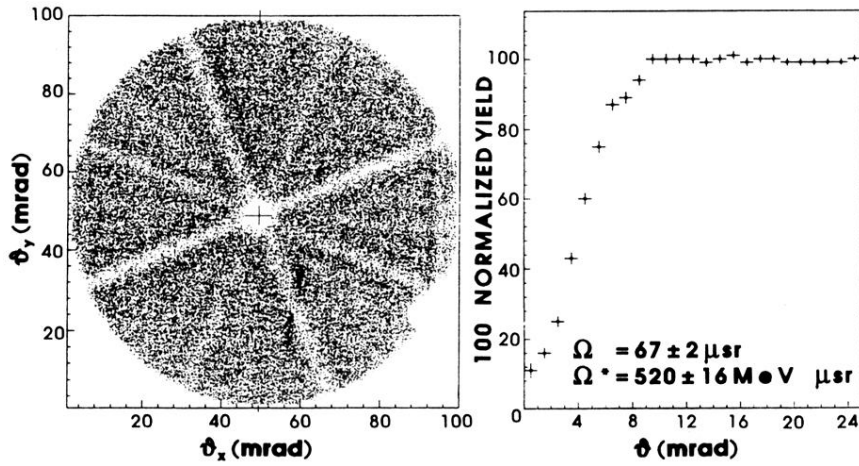


FIG. 2. Example of elastic (prompt) blocking dip, due to ^{32}S ions (124.2-MeV kinetic energy) on a Ni(100) crystal, 0.5 μm thick. Left: x - y scatter plot from the multiwire detector. Right: radial scan around the dip center.